Journal of the Physical Society of Japan **86**, 024705 (2017)
https://doi.org/10.7566/JPSJ.86.024705

Magnetic Moments and Ordered States in Pyrochlore Iridates $Nd_2Ir_2O_7$ and $Sm_2Ir_2O_7$ Studied by Muon-Spin Relaxation

Retno Asih[1,2,3*], Noraina Adam[1,4], Saidah Sakinah Mohd-Tajudin[1,4], Dita Puspita Sari[1,2,3], Kazuyuki Matsuhira[5], Hanjie Guo[1,6†], Makoto Wakeshima[7], Yukio Hinatsu[7], Takehito Nakano[2], Yasuo Nozue[2], Shukri Sulaiman[4], Mohamad Ismail Mohamed-Ibrahim[4], Pabitra Kumar Biswas[8‡], and Isao Watanabe[1,2,4,6,9§]

[1]*Advanced Meson Science Laboratory, RIKEN Nishina Center, Wako, Saitama 351-0198, Japan*
[2]*Department of Physics, Graduate School of Science, Osaka University, Toyonaka, Osaka 560-0043, Japan*
[3]*Department of Physics, Faculty of Mathematics and Natural Science, Institut Teknologi Sepuluh Nopember, Surabaya 60111, Indonesia*
[4]*Computational Chemistry and Physics Laboratory, School of Distance Education, Universiti Sains Malaysia, Penang 11800, Malaysia*
[5]*Faculty of Engineering, Kyushu Institute of Technology, Kitakyushu 804-8550, Japan*
[6]*Department of Physics and State Key Laboratory of Silicon Materials, Zhejiang University, Hangzhou 310027, China*
[7]*Division of Chemistry, Graduate School of Science, Hokkaido University, Sapporo 060-0810, Japan*
[8]*Bulk μSR Group, Paul Scherrer Institut, 5232 Villigen PSI, Switzerland*
[9]*Muon Spin Resonance Laboratory, Department of Condensed Matter Physics, Faculty of Science, Hokkaido University, Sapporo 060-0810, Japan*

(Received August 27, 2016; accepted November 28, 2016; published online January 13, 2017)

Magnetic-ordered states of the pyrochlore iridates $Nd_2Ir_2O_7$ (Nd227) and $Sm_2Ir_2O_7$ (Sm227), showing metal–insulator transitions at 33 and 117 K, respectively, were studied by both the muon-spin-relaxation (μSR) method and density functional theory (DFT) calculations. A long-range magnetic ordering of Ir moments appeared in conjunction with the metal insulator transition, and additional long-range-ordered states of Nd/Sm moments were confirmed at temperatures below about 10 K. We found that the all-in all-out spin structure most convincingly explained the present μSR results of both Nd227 and Sm227. Observed internal fields were compared with values derived from DFT calculations. The lower limits of the sizes of magnetic moments were estimated to be 0.12 μ_B and 0.2 μ_B for Ir and Nd moments in Nd227, and 0.3 μ_B and 0.1 μ_B for Ir and Sm moments in Sm227, respectively. Further analysis indicated that the spin coupling between Ir and Nd/Sm moments was ferromagnetic for Nd227 and antiferromagnetic for Sm227.

1. Introduction

Geometrical frustration provides an ideal platform to study the exotic electronic ground states of magnetic moments that have an antiferromagnetic interaction. The series of systems having a pyrochlore lattice structure with the corner-sharing tetrahedral lattices of magnetic atoms is an interesting example of geometrically frustrated systems. These systems show a variety of electronic states such as heavy-fermion behaviors,[1,2] superconductivity,[3] anomalous Hall effects,[4,5] metal–insulator transitions (MITs),[6,7] and a possible spin-liquid state.[8] One of these systems is the pyrochlore iridates, $R_2Ir_2O_7$ (R227, R = Nd, Sm, Eu, Gd, Tb, Dy, or Ho), which have the relatively large spin–orbit coupling (SOC) inherent in Ir 5d electrons and a d–f exchange interaction that has been suggested to lead to peculiar electronic properties.[9–11] R227 also show MITs at T_{MI}, which seem to be accompanied by magnetic transitions. T_{MI} gradually decreases from 141 K for R = Ho to 117 K for R = Sm with increasing ionic radius of the trivalent R. T_{MI} suddenly drops to 33 K for Nd227, and no MIT is observed in Pr227, which shows metallic behavior.[12–14]

The appearance of magnetically ordered states below T_{MI} has been confirmed by muon-spin relaxation (μSR) studies on some of the R227.[15–18] Clear muon-spin precession behavior is observed below T_{MI}, proving the appearance of a coherent magnetic long-range ordering (LRO). No muon-spin precession behavior and no signature of the appearance of static magnetic-ordered states are observed in Pr227 down to 25 mK.[19–21] Changing R, a frozen glassy state with small magnetic moments is observed in the case of R = Bi, which has a larger ionic radius than Pr.[22]

One important point in the investigation of the R227 series is to clarify how Ir moments order for different R and their relation to the MIT. This is because the Ir moment has a large SOC effect and is expected to play a key role in describing the intrinsic electronic properties of R227. Another important point is to study the effect of the d–f exchange interaction on the ordered state of Ir moments to obtain the magnetic phase diagram. In our previous paper on Nd227, we reported that the LRO of Ir moments appear in conjunction with the MIT at T_{MI} = 33 K.[18] The estimated internal field at the muon site caused by the only LRO of Ir moments is smaller than those observed in other R227, such as R = Yb, Y, and Eu.[15,17] This leads us to a previous conclusion that the Ir moment is reduced as the system changes from the insulating state to the metallic state. In addition to this LRO of Ir moments, another ordered state of Nd moments is observed below around 10 K. This Nd ordering enhances the internal field at the muon site. Since a pulsed muon beam was used for our previous study[18] at the RIKEN-RAL muon facility,[23] this additional internal field from Nd moments has not been clearly distinguished due to the limited time resolution of the muon detection system and should be investigated by DC muon beams with a higher time resolution. In addition to Nd227, the magnetic properties of Sm227 are still unclear. Although the result of a μSR study on Sm227 has already been reported,[24] the MIT of the sample was not clear and the sample was slightly conducting even below T_{MI}, which was lower than that observed in other reports (T_{MI} = 117 K).[13,14] The estimated

magnetic transition temperature ($T_N = 70$ K) is not consistent with T_{MI} suggesting the lack of an LRO.[24] This may be due to the difficulty of the preparation of samples.

Since Sm227 is the neighbor to Nd227, it is important to restudy this system to clarify the novel electronic states of *R*227 by μSR using samples having clear MITs with well-defined T_{MI}. Until now, important magnetic properties such as spin structures and the sizes of magnetic moments have not been well clarified because the Ir moment is expected to be very small and because Ir is a good neutron absorber similarly to other *R* elements such as Sm and Nd. A neutron experiment estimated the size of the magnetic moment of Nd,[25] but this study did not include the effect of the *d*–*f* exchange interaction due to the lack of the scattering signal from the Ir moment. μSR is a sensitive and useful microscopic magnetic probe for investigating the static and dynamic properties of small and neutron-insensitive magnetic moments. Numerous μSR studies have already revealed novel electronic states in many frustrated systems.[26–32] It is obvious from past μSR studies that μSR can clearly sense the appearance of LRO in *R*227.[15–18,24] Recently, we have been trying to clarify spin structures by using μSR data in conjunction with density functional theory (DFT) calculations. When muon-spin precession is observed, precession frequencies give us information of internal fields originating from the surrounding magnetic moments at muon sites. These internal fields are estimated on the basis of the dipole–dipole interaction between muon spins and surrounding magnetic moments. Such combined studies involving experimental and computational techniques can allow us to discuss the spin structures in magnetic-ordered states including the effect of the *d*–*f* exchange interaction, which is still unclear and needs to be investigated. Accordingly, we carried out μSR and DFT calculations on both Nd227 and Sm227 systems in order to understand the change in the Ir magnetic moment.

2. Procedure

Polycrystalline samples of Nd227 and Sm227 were synthesized by the solid-reaction method.[13,14] Both samples were firstly verified to be in a single phase by X-ray diffraction measurement. Resistivity measurements on the samples were performed before the μSR study in order to evaluate the sample quality. The T_{MI} was confirmed by the resistivity measurements using the standard four-probe method to be 33 K for Nd227 and 117 K for Sm227. The MIT behavior was the same as that previously reported, indicating that our used samples also had the same quality as those used in previous studies.[13,14,18,25] The μSR study was carried out in the DOLLY area at the Paul Scherrer Institut (PSI) in Switzerland. A continuous surface-muon beam was used in order to observe fast muon-spin precession, which was not observed by using pulsed muon beams at RIKEN-RAL. The asymmetry parameter, $A(t)$ (μSR time spectrum), is defined as $A(t) = [F(t) - \alpha B(t)]/[F(t) + \alpha B(t)]$, where $F(t)$ and $B(t)$ are the numbers of muons detected by forward and backward counters, which are aligned upstream and downstream of the sample along the beam line, respectively. α is a parameter used to geometrically compensate the numbers of muons counted by the forward and backward counters. The time evolution of $A(t)$ was measured up to about 8 µs under the zero-field (ZF) condition, for which the time resolution is about 30 times higher rather than that used at RIKEN-RAL.

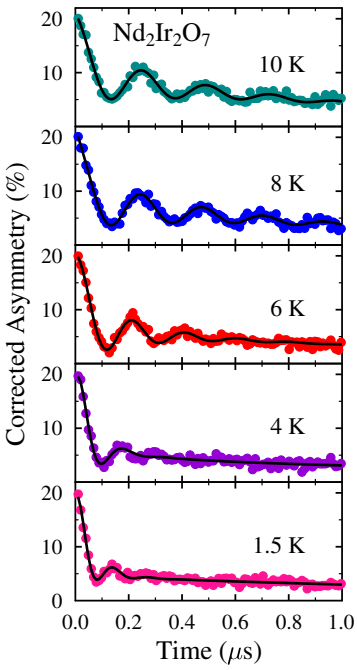

Fig. 1. (Color online) Zero-field μSR time spectra of $Nd_2Ir_2O_7$ measured at several temperatures below $T_{MI} = 33$ K. Clear muon-spin precession was observed down to 1.5 K. Solid lines are the best-fit results obtained using Eq. (1). The precession frequency seems to increase with decreasing temperature, showing the increase in the internal field at the muon sites.

DFT and dipole-field calculations were conducted in RIKEN by using a cluster supercomputing system named HOKUSAI Greatwave. The electrostatic potential was estimated in both Nd227 and Sm227 by using the computational program of the Vienna Ab initio Simulation Package (VASP).[33,34] The plane wave approximation and pseudo-potential method were used for DFT calculations. Dipole-field calculations to estimate the internal fields at the muon sites were carried out taking into account the spherical volume with 100 Å radius surrounding the muon.

3. Results

3.1 $Nd_2Ir_2O_7$

Figure 1 displays ZF-μSR time spectra measured at lower temperatures below $T_{MI} = 33$ K. Clear muon-spin precession was observed down to 1.5 K. The precession frequency increased and the precession amplitude decreased as the temperature decreased below 10 K. Accordingly, it was confirmed from the observation of the clear muon-spin precession behavior that Nd moments indeed undergo LRO below about 10 K. This result is clear confirmation of the suggestion from the neutron scattering experiment[25] as discussed in our previous study.[18]

The time spectra were analyzed by using the following function, and the internal field at the muon site was estimated.

$$A_{(t)} = A_1 e^{-\lambda_1 t} + A_2 e^{-\lambda_2 t} \cos(\omega t + \phi) + A_3 e^{-\lambda_3 t} \qquad (1)$$

The first component expresses the slowly relaxing behavior beyond 1 µs. The fitting quality of this component was the same as that of Fig. 1(a) in our previous paper.[18] The second

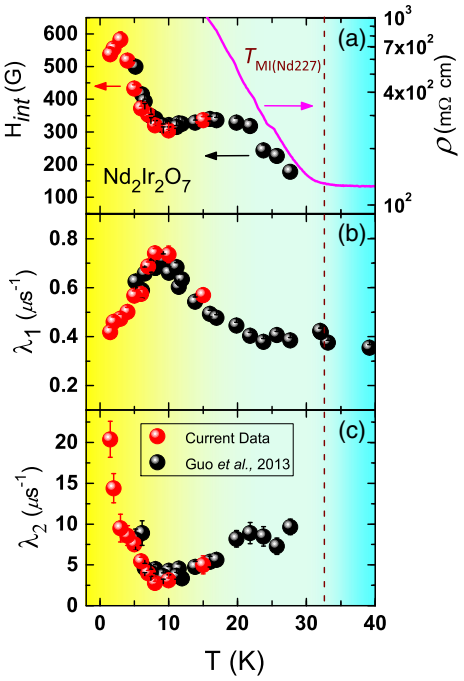

Fig. 2. (Color online) Temperature dependence of (a) internal field at the muon site, $H_{\rm int}$, (b) slow relaxation rate, λ_1, and (c) damping rate of the muon-spin precession, λ_2, obtained from the analysis of the ZF-μSR time spectra of $Nd_2Ir_2O_7$ by applying Eq. (1). Red/light marks are the analysis results obtained in the current study and black/dark ones were obtained in our previous study.[18] The broken line indicates $T_{\rm MI}$ (= 33 K). The Nd moments undergo LRO below about 10 K, as suggested by the neutron scattering experiment.[25] The area at $T > T_{\rm MI}$ indicates the paramagnetic region. The temperature dependence of the resistivity of this sample is also displayed in (a) by the solid line as a reference of the MIT.[13,14]

component expresses the muon-spin precession. The third one describes the fast-relaxing component of the time spectrum observed in the earlier time region within 0–0.1 µs. A_1, A_2, and A_3 are the initial asymmetries at $t = 0$. λ_1 and λ_3 are the relaxation rates of the slow- and fast-relaxing components, respectively. λ_2, ω, and ϕ are the damping rate, precession frequency and phase of the muon-spin precession, respectively. The internal field at the muon site, $H_{\rm int}$, was calculated from ω by using the equation $\omega = \gamma_\mu H_{\rm int}$, where γ_μ is the gyromagetic ratio of the muon spin ($2\pi \times 13.55$ kHz/G). The solid lines in Fig. 1 are the best-fit results subtracting the small background components, which originate from muons surrounding the sample.

Figure 2 exhibits the temperature dependences of the extracted parameters from the analysis of the ZF-μSR time spectra. In addition to the analysis results of the current study (red/light marks), our previous data measured at RIKEN-RAL are also displayed (black/dark marks).[18] The analysis results are in good agreement with those obtained at RIKEN-RAL. The temperature dependence of the resistivity of the sample measured in this study is also indicated in Fig. 2. The clear change in the resistivity at $T_{\rm MI}$ (= 33 K) is shown by the broken line. $H_{\rm int}$ shown in Fig. 2(a) starts to increase just below $T_{\rm MI}$ and tends to saturate between 20 and 10 K. The error bars of $H_{\rm int}$ in this temperature range are about the same size as the symbols. Then, $H_{\rm int}$ increases again with decreasing temperature and saturates below about 5 K. The second increase in $H_{\rm int}$ was due to the appearance of additional LRO of Nd moments. The saturated internal field

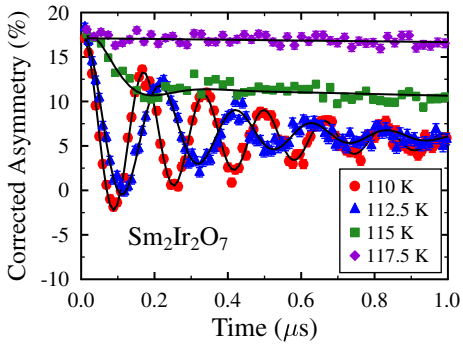

Fig. 3. (Color online) ZF-μSR time spectra of $Sm_2Ir_2O_7$ measured at various temperatures. Clear muon-spin precession behavior is observed just below 117 K, which is the same as $T_{\rm MI}$. The precession frequency and the amplitude are much larger than those observed in $Nd_2Ir_2O_7$, indicating that the internal field at the muon sites is larger and that the spin alignment is more coherent than those of $Nd_2Ir_2O_7$. Solid lines are the best-fit results obtained using Eq. (1).

was determined to be about 530 G. This value was almost the same as that estimated in our previous study from the μSR measurement in a longitudinal field (LF) applied along the initial muon-spin direction.[18] Since $H_{\rm int}$ increased when Nd moments underwent LRO, the direction of the dipole field from the Nd moments at the muon site is parallel to that caused by the LRO of Ir moments. The additional field caused by Nd moments was about 260 G.

λ_1 indicated in Fig. 2(b) shows a peak around 10 K in its temperature dependence and decreases with decreasing temperature below 10 K. This behavior can be understood to be due to the slowing-down behavior of the Nd moments that appeared around 10 K when Nd moments underwent LRO. λ_2 tends to increase with decreasing temperature below about 10 K. This parameter reflects the degree of the distribution of the internal field at the muon site in LRO. Therefore, the increase in λ_2 means that the coherency of the alignment of Nd moments is relatively deformed compared with that of Ir moments.

3.2 *$Sm_2Ir_2O_7$*

Figure 3 displays ZF-μSR time spectra of $Sm_2Ir_2O_7$ measured at various temperatures. Above $T_{\rm MI} = 117$ K, the time spectrum is almost flat within the time region of 0–1 µs. This flat time spectrum means that the muon-spin polarization is slowly relaxing and no strong internal field exists at the muon sites. This slow relaxation behavior is considered to be mainly caused by dynamic thermal fluctuation of Sm moments. With decreasing temperature, the time spectrum rapidly changes just below $T_{\rm MI}$, and the fast-relaxing behavior appears within 0–0.2 µs. With further decreasing temperature, clear muon-spin precession behavior is observed. Therefore, it is clear that LRO occurred in Sm227 in conjunction with the MIT, as observed in Nd227. Since this tendency is also observed in other *R*227, the appearance of LRO in conjunction with the MIT is a common characteristic electronic property in the series of *R*227. The amplitude of the muon-spin precession was larger than that of Nd227. This means that the coherent length of the magnetic order in Sm227 is larger than that in Nd227. Since no fast relaxation behavior was observed, the analysis function of Eq. (1) excluding the third component was used for the analysis of

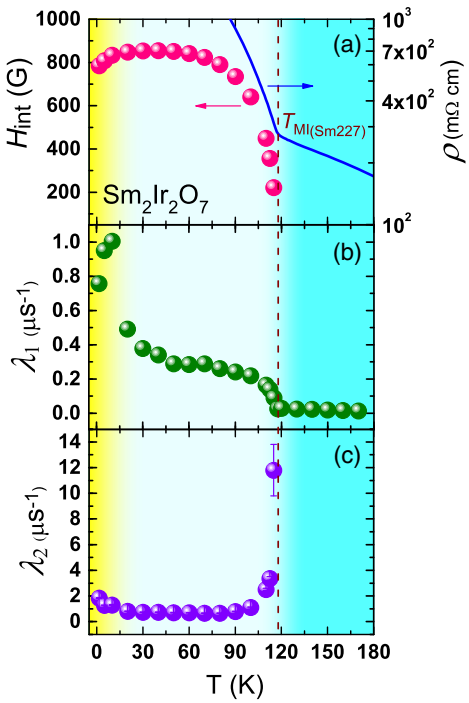

Fig. 4. (Color online) Temperature dependences of (a) internal field at the muon sites, H_{int}, (b) slow relaxation rate, λ_1, and (c) damping rate of the muon-spin precession, λ_2. These parameters were obtained from the analysis of the ZF-μSR time spectra of $Sm_2Ir_2O_7$ by using Eq. (1). The broken line indicates T_{MI} (= 117 K).[13] The Sm moments undergo LRO below about 10 K. The area at $T > T_{MI}$ indicates the paramagnetic region. The temperature dependence of the resistivity of this sample is also displayed in (a) by the solid line as a reference of the MIT.

the time spectra in the case of Sm227. The solid lines in Fig. 3 are the best-fit results.

Figure 4 shows the temperature dependences of the extracted parameters from the analysis, drawn in the same manner as in the case of Nd227. The temperature dependence of the resistivity of the sample measured in this study is also indicated in Fig. 4. The clear change in the resistivity at T_{MI} (= 117 K) is shown by the broken line. The existence of a well-defined T_{MI} indicates the same quality of this sample as those reported in previous studies.[13,14] H_{int} displayed in Fig. 4(a) starts to increase just below T_{MI} and tends to saturate below about 60 K. This saturation in H_{int} below T_{MI} was the same as that observed in Nd227. The saturated H_{int} was about 830 G. With further decreasing temperature, H_{int} decreases again below about 10 K. The decrease in H_{int} was in the opposite direction compared with the case of Nd227. λ_1 remains constant with a small value above T_{MI} and suddenly increases below T_{MI}. No critical slowing-down behavior was observed at T_{MI}. This was also the same behavior as that of Nd227.[18] After λ_1 gradually increases with decreasing temperature below T_{MI}, λ_1 is markedly enhanced below about 20 K and shows a peak at about 10 K. λ_2 remains nearly constant below T_{MI} and slightly increases below about 20 K.

4. Discussion

4.1 Comparison of H_{int} between Nd227 and Sm227

While the LRO of Ir and Nd moments in Nd227 was clarified and discussed in our previous study,[18] clear evidence of the occurrence of LRO of the Nd moments in a sea of coherently aligned Ir moments was obtained in the current study by observing clear muon-spin precession behavior even below 10 K. This means that even though Ir moments showed LRO just below T_{MI} in Nd227, Nd moments still dynamically fluctuate down to 10 K. Thus, the triggering mechanism of the magnetic ordering of Ir moments is not due to the ordering of Nd moments, but is caused by the MIT.

It should be noted that the additional internal field originating from the ordered Nd moments at the muon sites is in the same direction as that induced by Ir moments because H_{int} increases when the LRO of Nd moments appears. In contrast, H_{int} in Sm227 decreases below about 10 K. This difference in H_{int} leads to the same conclusion as that obtained from the discussion for the case of Nd227[18] that only Ir moments undergo LRO below T_{MI} in Sm227 and that Sm moments are still fluctuating in the sea of coherently ordered Ir moments. The enhancement in λ_1 around 10 K, as shown in Fig. 4(b), is therefore regarded as the appearance of the slowing-down behavior of Sm moments toward LRO below 10 K, and the LRO of Sm moments creates additional internal fields at the muon sites, which was also observed in Nd227. Even so, there are some differences. One is that the saturated H_{int} in Sm227, which originates from only the Ir moments, was about 2.5 times as large as that of Nd227. The other is that the change in H_{int} below about 10 K is in the opposite direction to that of Nd227. The former result simply indicates that the Ir moments in Nd227 is smaller than that in Sm227. The latter result means that the direction of the additional internal field at the muon sites originating from the ordered Sm moments is opposite to that of the internal field originating from the ordered Ir moments. This suggests that the spin coupling between Sm and Ir moments is opposite to that of Nd227.

4.2 Estimation of muon stopping sites by DFT calculations

As the next step, we discuss the sizes of magnetic moments and the spin alignments of Ir, Nd, and Sm from the current μSR study. In order to do this, the most important information is the muon stopping sites in Nd227 and Sm227. An injected muon is considered to initially stop at minimum-potential positions in the crystal because it has a positive charge.[35–37] An example of the expected muon-stopping positions in pylochrore systems was first reported by Foronda et al. for $Pr_2B_2O_7$ (B = Sn, Zr, Hf).[38] They suggested that muons stop near an oxygen atom, which is located in the center of the R tetrahedra. This is because an injected muon has a positive charge and preferentially stops close to anions, which have negative charges.

Initial muon stopping positions can be predicted by estimating the minimum-potential positions from DFT calculations.[35–37] Figure 5 shows the minimum-potential positions in both Nd227 and Sm227 estimated from our DFT calculations. These positions are located on the trigonal symmetry axis and outside of the R tetrahedra. As can be easily seen, the initial stopping positions are similar in both Nd227 and Sm227 but are different from those suggested from the previous μSR study on $Pr_2B_2O_7$ (B = Sn, Zr, Hf).[38] The potential distribution in $Pr_2B_2O_7$ is expected to be different from that of Nd227 and Sm227 due to the different ionic sizes of the composing elements, causing a change in

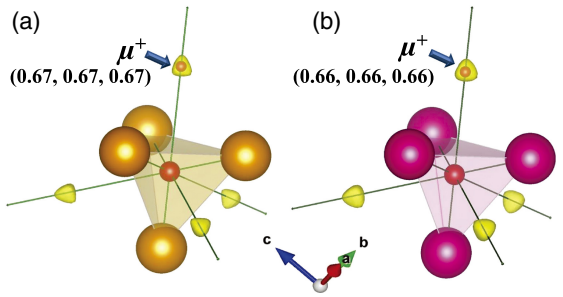

Fig. 5. (Color online) Minimum-potential regions, which were estimated from DFT calculations, (a) in $Nd_2Ir_2O_7$ and (b) $Sm_2Ir_2O_7$. The tetrahedral structures composed of Nd/Sm (yellow/purple large balls) and O (red small balls) atoms are shown. The four trigonal symmetry axes of the *R*-tetrahedron are also shown by solid lines. Isosurface areas indicate the regions with energy 100 meV higher than that at the minimum-potential positions. The exact minimum-potential positions are highlighted by dark color in the isosurface areas.

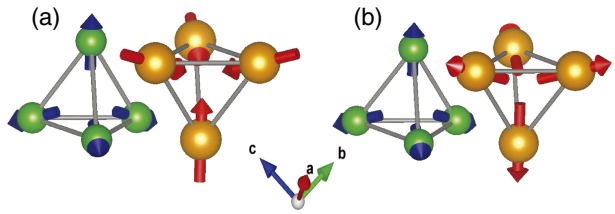

Fig. 6. (Color online) Possible couplings of Ir spins with Nd/Sm spins in the case of the all-in all-out spin structure. These models were used for DFT calculations in the current study. (a) Antiferromagnetic coupling and (b) ferromagnetic coupling.

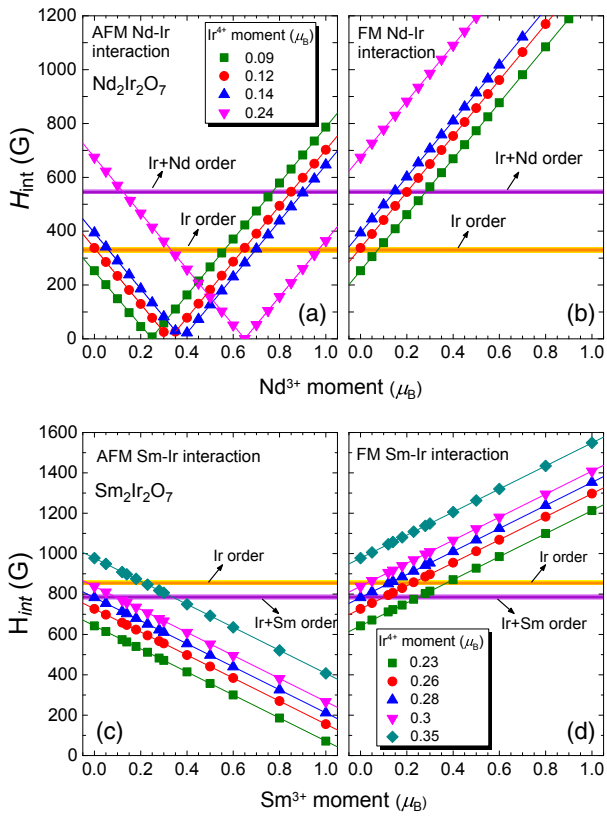

Fig. 7. (Color online) Simulation results of the saturated H_{int} taking into account only dipole fields from the Ir and Nd/Sm moments in (a, b) Nd227 and (c, d) Sm227. The spin coupling between Ir and Nd/Sm is antiferromagnetic (a, c) and ferromagnetic (b, d). These couplings are shown in Fig. 6. The values of H_{int} from the Ir and Nd/Sm moments were calculated independently.

possible muon positions. More detailed DFT calculations are currently being performed to determine the difference in muon stopping positions.

4.3 Spin structures and magnetic moments of Nd227 and Sm227

Assuming local minimum-potential positions as the muon stopping sites, H_{int} values were simulated in order to discuss the spin structures in Nd227 and Sm227. We examined the cases of the all-in all-out and two-in–two-out spin structures for both Ir and Nd/Sm spins. These structures are considered to be realized from the view point of the pyrochlore structure, while the all-in all-out spin structure is strongly indicated from the results of neutron scattering[25] and X-ray measurements.[39] Antiferromagnetic and ferromagnetic spin couplings between the Ir and Nd/Sm tetrahedra were also examined. These couplings are displayed in Fig. 6.

First, H_{int} at the position suggested by Foronda et al. was examined. It was found that neither the spin structures nor the couplings successfully explained our current results. In particular, the saturated H_{int} from only Ir moments was calculated to be very small at this position even though a possible maximum magnetic moment of $1\,\mu_B$ was assumed on Ir. Since this suggested position seems to be reasonably symmetric with surrounding Ir moments, H_{int} from the Ir moments should be fairly well canceled. Accordingly, H_{int} was examined by assuming our estimated muon positions shown in Fig. 5. Firstly, the two-in–two-out spin structure was examined. It was found that this spin structure could not explain our current results well. This was due to cancellations of dipole fields caused by anti-parallel spin directions within the Ir and Nd/Sm tetrahedra.

Secondly, the all-in all-out spin structure was investigated taking into account H_{int} from the Ir and Nd/Sm moments independently. Figures 7(a) and 7(b) show the simulation results for the antiferromagnetic and ferromagnetic spin coupling in the case of Nd227, respectively. The size of the Ir moments changed from 0.09 to $0.24\,\mu_B$ as the size of the Nd moments changed from zero to $0.8\,\mu_B$. H_{int} from the only Ir moments (about 320 G) is indicated at the zero value in the Nd moments. Then, the size of the Ir moments was estimated to be $0.12\,\mu_B$ in order to explain the observed value. The increase in the size of the Nd moments reproduced the change in H_{int} below about 10 K.

The experimental results of the saturated H_{int} at around 20 and 1.5 K are also shown in Fig. 7 by solid lines (the lower line is for only Ir and the upper line is for both Ir and Nd). The width of the solid lines indicates the width of the data scattering, which was estimated by eye from Fig. 2(a). In the case of the antiferromagnetic coupling, H_{int} decreases with increasing size of the Nd moments from zero. This means that the direction of the H_{int} component from the Nd moments is opposite to that from the Ir moments. This result does not match the experimental result, which shows an increase in H_{int} when LRO appears and the size of the Nd moments is increasing below about 10 K. On the other hand, H_{int} increases linearly with increasing size of the Nd moments in the case of the ferromagnetic coupling. This

tendency matches the current μSR results and also supports the prediction suggested from the neutron scattering experiment.[25] Accordingly, the possible size of the Nd moments was estimated from Fig. 7(b) to be about $0.2\,\mu_B$ in the ground state. This value can be obtained from the intersection between the experimental and simulated values.

The same method was applied to the case of Sm227. The simulation results of the saturated H_{int} in the case of Sm227 with the antiferromagnetic and ferromagnetic spin coupling are shown in the Figs. 7(c) and 7(d), respectively. As can be seen in Fig. 4(a), the direction of the H_{int} component from the Sm moments is opposite to that from the Ir moments and tends to cancel H_{int} as the size of the Sm moments increases. Therefore, the antiferromagnetic spin coupling more convincingly explains the experimental results. Following the same logic as that used in the case of Nd227, we estimated the size of the Ir and Sm moments to be about $0.3\,\mu_B$ and $0.1\,\mu_B$, respectively. As a result, we can conclude from the current study that the size of the Ir moments decreases by more than a half when R changes from Sm to Nd, although the Ir moments was suggested to remain at $0.5\,\mu_B$, even in Nd227 from the previous DFT calculations.[40]

Finally, it should be noted that these estimated magnetic moments are lower-limit values. In the case of strongly hybridized systems, magnetic moments are expected to be spatially distributed around the nuclear position through the hybridization with electronic orbitals of surrounding anions.[41] This spatial distribution reduces H_{int} due to the cancellation effect of dipole fields originating from symmetric positions around the nuclear position. In addition, the stopping muon itself will cause local deformation of the crystal structure, resulting in the relaxation of the muon position.[38,42] This local effect sometimes modifies the electronic state around the muon and reduces the size of the magnetic moment nearest to the muon.[42] Recently, it has also been pointed out that the existence probability of the muon itself is spread around the local minimum position due to the self-zero-point vibration motion, which is a character of a fine particle.[35] These local and quantum effects caused by the injected muon reduce H_{int}. This means that the magnetic moments of Ir, Nd, and Sm estimated in the current study on the basis of the simple point-dipole estimation are underestimated and are the *average lower limits* of realistic values. However, even taking into account these local effects, the all-in all-out spin structure and the spin couplings between the Ir and Nd/Sm tetrahedra do not change. It should also be noted that our current result is the first experimental estimation of the possible sizes of magnetic moments of Nd, Sm and Ir that includes the effect of the *d–f* exchange interaction. Advanced DFT calculations taking into account these local and quantum effects are on going and will be reported separately.

5. Summary

Zero-field μSR measurements were performed on $Nd_2Ir_2O_7$ (Nd227) and $Sm_2Ir_2O_7$ (Sm227) in order to investigate their spin structures and magnetic moments. In the case of Nd227, the additional LRO of the Nd moments was confirmed below about 10 K. The saturated internal field at the muon sites, H_{int}, which originates from both Ir and Nd orderings, was accurately estimated to be about 530 G. In the case of Sm227, the LRO of the Ir moments appeared just below the metal–insulator transition temperature, $T_{MI} = 117$ K, as well as in the case of Nd227. The additional LRO of the Sm moments appeared below about 10 K. This result clearly demonstrates that the appearance of the LRO of the Ir moments is a common electronic property of the $R_2Ir_2O_7$ system and is triggered in conjunction with the metal–insulator transition. In the case of Sm227, H_{int} increased with decreasing temperature below T_{MI} and saturated below about 60 K with a value of about 830 G. In contrast to the case of Nd227, H_{int} decreased with decreasing temperature when the Sm moments started to undergo LRO below 10 K. The all-in all-out spin structure within the Ir and Nd/Sm tetrahedra was confirmed to be realistic from the DFT and dipole-field calculations. The magnetic moments of Ir, Nd, and Sm were estimated to be Ir $= 0.12\,\mu_B$ and Nd $= 0.2\,\mu_B$ for Nd227, and Ir $= 0.3\,\mu_B$ and Sm $= 0.1\,\mu_B$ for Sm227. The spin couplings between Ir and Nd/Sm were found to be ferromagnetic for Nd227 and antiferromagnetic for Sm227. We conclude that the magnetic moment of Ir^{4+} shrinks by more than a half when the rare-earth metal is changed from Sm to Nd.

Acknowledgments

The authors would like to thank the staff of the bulk-muon group of PSI for supporting the current μSR experiment at PSI. We thank Dr. Tomiyasu and Dr. Onoda for valuable discussions concerning the size and spin structure of Nd227 and Sm227. This study was supported by the MEXT/JSPS KAKENHI Grant Number 15H03692, the RIKEN Junior Research Associate (JRA) Program, and the Indonesian scholarship program Lembaga Pengelola Dana Pendidikan (LPDP).

*retno@nano.phys.sci.osaka-u.ac.jp
†Present address: Max-Planck-Institute for Chemical Physics of Solids, Physics of Correlated Matter, Dresden 01187, Germany
‡Present address: ISIS Facility, STFC Rutherford Appleton Laboratory, Didcot OX11 0QX, U.K.
§nabedon@riken.jp

1) Y. Matsushita, H. Ueda, and Y. Ueda, Nat. Mater. **4**, 845 (2005).
2) M. Shiga, K. Fujisawa, and H. Wada, J. Phys. Soc. Jpn. **62**, 1329 (1993).
3) M. Hanawa, Y. Muraoka, T. Tayama, T. Sakakibara, J. Yamaura, and Z. Hiroi, Phys. Rev. Lett. **87**, 187001 (2001).
4) Y. Taguchi, Y. Oohara, H. Yoshizawa, N. Nagaosa, and Y. Tokura, Science **291**, 2573 (2001).
5) Y. Machida, S. Nakatsuji, Y. Maeno, T. Tayama, T. Sakakibara, and S. Onoda, Phys. Rev. Lett. **98**, 057203 (2007).
6) A. W. Sleight, J. L. Gilison, J. F. Weiher, and W. Bindloss, Solid State Commun. **14**, 357 (1974).
7) A. Yamamoto, P. S. Sharma, Y. Okamoto, A. Nakao, H. Aruga-Katori, S. Niitaka, D. Hashizume, and H. Takagi, J. Phys. Soc. Jpn. **76**, 043703 (2007).
8) S. T. Bramwell and M. J. P. Gingras, Science **294**, 1495 (2001).
9) G. Chen and M. Hermele, Phys. Rev. B **86**, 235129 (2012).
10) X. Wan, A. M. Turner, A. Vishwanath, and S. Y. Savrasov, Phys. Rev. B **83**, 205101 (2011).
11) X. Wan, A. Vishwanath, and S. Y. Savrasov, Phys. Rev. Lett. **108**, 146601 (2012).
12) D. Yanagishima and Y. Maeno, J. Phys. Soc. Jpn. **70**, 2880 (2001).
13) K. Matsuhira, M. Wakeshima, R. Nakanishi, T. Yamada, A. Nakamura, W. Kawano, S. Takagi, and Y. Hinatsu, J. Phys. Soc. Jpn. **76**, 043706 (2007).
14) K. Matsuhira, M. Wakeshima, Y. Hinatsu, and S. Takagi, J. Phys. Soc. Jpn. **80**, 094701 (2011).

15) S. Zhao, J. M. Mackie, D. E. MacLaughlin, O. O. Bernal, J. J. Ishikawa, Y. Ohta, and S. Nakatsuji, Phys. Rev. B **83**, 180402(R) (2011).
16) S. M. Disseler, C. Dhital, T. C. Hogan, A. Amato, S. R. Giblin, C. de la Cruz, A. Daoud-Aladine, S. D. Wilson, and M. J. Graf, Phys. Rev. B **85**, 174441 (2012).
17) S. M. Disseler, C. Dhital, A. Amato, S. R. Giblin, C. de la Cruz, S. D. Wilson, and M. J. Graf, Phys. Rev. B **86**, 014428 (2012).
18) H. Guo, K. Matsuhira, I. Kawasaki, M. Wakeshima, Y. Hinatsu, I. Watanabe, and Z. A. Xu, Phys. Rev. B **88**, 060411(R) (2013).
19) S. Nakatsuji, Y. Machida, Y. Maeno, T. Tayama, T. Sakakibara, J. van Duijn, L. Balicas, J. N. Millican, R. T. Macaluso, and J. Y. Chan, Phys. Rev. Lett. **96**, 087204 (2006).
20) D. E. MacLaughlin, Y. Ohta, Y. Machida, S. Nakatsuji, G. M. Luke, K. Ishida, R. H. Heffner, L. Shu, and O. O. Bernal, Physica B **404**, 667 (2009).
21) D. E. MacLaughlin, Y. Nambu, Y. Ohta, Y. Machida, S. Nakatsuji, and O. O. Bernal, J. Phys.: Conf. Ser. **225**, 012031 (2010).
22) P. J. Baker, J. S. Moller, F. L. Pratt, W. Hayes, S. J. Blundell, T. Lancaster, T. F. Qi, and G. Cao, Phys. Rev. B **87**, 180409(R) (2013).
23) K. Nagamine, T. Matsuzaki, K. Ishida, I. Watanabe, R. Kadono, G. H. Eaton, H. J. Jones, G. Thomas, and W. G. Williams, Hyperfine Interactions **87**, 1091 (1994).
24) M. J. Graf, S. M. Disseler, C. Dhital, T. Hogan, M. Bojko, A. Amato, H. Luetkens, C. Baines, D. Margineda, S. R. Giblin, M. Jura, and S. D. Wilson, J. Phys.: Conf. Ser. **551**, 012020 (2014).
25) K. Tomiyasu, K. Matsuhira, K. Iwasa, M. Watahiki, S. Takagi, M. Wakeshima, Y. Hinatsu, M. Yokoyama, K. Ohoyama, and K. Yamada, J. Phys. Soc. Jpn. **81**, 034709 (2012).
26) A. P. Ramirez, G. P. Espinosa, and A. S. Cooper, Phys. Rev. Lett. **64**, 2070 (1990); A. P. Ramirez, G. P. Espinosa, and A. S. Cooper, Phys. Rev. B **45**, 2505 (1992).
27) A. Keren, L. P. Le, G. M. Luke, W. D. Wu, Y. J. Uemura, Y. Ajiro, T. Asano, H. Huriyama, M. Mekata, and H. Kikuchi, Hyperfine Interactions **85**, 181 (1994).
28) Y. J. Uemura, A. Keren, K. Kojima, L. P. Le, G. M. Luke, W. D. Wu, Y. Ajiro, T. Asano, Y. Kuriyama, M. Mekata, H. Kikuchi, and K. Kakurai, Phys. Rev. Lett. **73**, 3306 (1994).
29) S. R. Dunsiger, R. F. Kiefl, K. H. Chow, B. D. Gaulin, M. J. P. Gingras, J. E. Greedan, A. Keren, K. Kojima, G. M. Luke, W. A. MacFarlane, N. P. Raju, J. E. Sonier, Y. J. Uemura, and W. D. Wu, Phys. Rev. B **54**, 9019 (1996).
30) A. Keren, K. Kojima, L. P. Le, G. M. Luke, W. D. Wu, Y. J. Uemura, M. Takano, H. Dabkowska, and M. J. P. Gingras, Phys. Rev. B **53**, 6451 (1996).
31) I. Watanabe, N. Wada, H. Yano, T. Okuno, K. Awaga, S. Ohira, K. Nishiyama, and K. Nagamine, Phys. Rev. B **58**, 2438 (1998).
32) F. L. Pratt, P. J. Baker, S. J. Blundell, T. Lancaster, S. Ohira-Kawamura, C. Baines, Y. Shimizu, K. Kanoda, and I. Watanabe, Nature **471**, 612 (2011).
33) G. Kresse and J. Furthmuller, Phys. Rev. **54**, 11169 (1996).
34) G. Kresse and J. Furthmüller, Comput. Mater. Sci. **6**, 15 (1996).
35) F. Bernardini, P. Bonfá, S. Massidda, and R. De Renzi, Phys. Rev. B **87**, 115148 (2013).
36) B. Adiperdana, E. Suprayoga, N. Adam, S. S. Mohd-Tajudin, A. F. Rozlan, S. Sulaiman, M. I. Mohamed-Ibrahim, T. Kawamata, T. Adachi, I. A. Dharmawan, R. E. Siregar, Y. Koike, and I. Watanabe, J. Phys.: Conf. Ser. **551**, 012051 (2014).
37) I. Watanabe, E. Suprayoga, N. Adam, S. S. Mohd-Tajudin, A. F. Rozlan, D. Puspita, R. Asih, F. Astuti, M. D. Umar, J. Angel, S. Sulaiman, and M. I. Mohamed-Ibrahim, Mater. Sci. Forum **827**, 347 (2015).
38) F. R. Foronda, F. Lang, J. S. Moller, T. Lancaster, A. T. Boothroyd, F. L. Pratt, S. R. Giblin, D. Prabhakaran, and S. J. Blundell, Phys. Rev. Lett. **114**, 017602 (2015).
39) C. Donnerer, M. C. Rahn, M. Moretti Sala, J. G. Vale, D. Pincini, J. Strempfer, M. Krisch, D. Prabhakaran, A. T. Boothroyd, and D. F. McMorrow, Phys. Rev. Lett. **117**, 037201 (2016).
40) H. Zhang, K. Haule, and D. Vanderbilt, arXiv:1505.01203v1.
41) A. C. Walters, T. G. Perring, J. S. Caux, A. T. Savici, G. D. Gu, C. C. Lee, W. Ku, and I. A. Zalizinyak, Nat. Phys. **5**, 867 (2009).
42) H. U. Suter, E. P. Stoll, and P. F. Meier, Physica B **326**, 329 (2003).